Pergamon

Int. J. Solids Structures Vol. 31, No. 5, pp. 711–732, 1994
Elsevier Science Ltd
Printed in Great Britain
0020-7683/94 $6.00 + .00

INTERMEDIATELY STIFFENED PLATES IN UNIAXIAL COMPRESSION

K. H. HOON
School of Mechanical and Production Engineering, Nanyang Technological University, Nanyang Avenue, Singapore 2263

and

J. RHODES
Department of Mechanical Engineering, University of Strathclyde, Glasgow G1 1XJ, United Kingdom

(*Received* 2 *June* 1992; *in revised form* 18 *August* 1993)

Abstract—A theoretical analysis is presented for the behaviour after buckling of intermediately stiffened plates loaded in compression. The loaded and unloaded edges are simply supported but the unloaded edges are free to wave in the plane of the plates. A semi-energy method of analysis, based on the von Karman's compatibility equation and the principle of minimum total potential energy, is used. The results are presented graphically for a range of plate aspect ratios and stiffener sizes and comparison is made with experimental results.

NOTATION

a	length of plate
b_s, d	stiffener flange width and depth, respectively
t	plate thickness
w	width of plate subelement
D	plate flexural rigidity $= Et^3/12(1-\nu^2)$
E	Young's modulus of elasticity $= 205\,000$ N mm^{-2}
$\bar{P}$	non dimensional value of load P applied to plate $= 2Pw/\pi^2 D$
$\bar{P}_{cr}$	non dimensional critical buckling load
x, y	Cartesian co-ordinates
u, v	in-plane displacements in the x and y directions, respectively
u^*	end displacement at the centroidal axis
$\bar{U}$	non-dimensional end displacement $[4u^*w^2E/\pi^2 aD]$
ε_x, ε_y	membrane strains at a point in the plate in the x and y directions
γ_{xy}	shear strain in the x–y plane
σ_x, σ_y	membrane stresses at a point in the plate in the x and y directions
τ_{xy}	shear stress in the x–y plane
ν	Poisson's ratio, taken as 0.3.

Other symbols are defined when they first appear. Primes denote differentiation in the y-direction, e.g. $\partial^2 Y/\partial y^2$.

INTRODUCTION

A thin steel plate is very flexible when it carries loads which act in the direction of its normal, but it is extremely stiff when the loads are applied within its plane. It is this rigidity that is utilised in the design of thin-walled structures. With these structures, the plates, which form the structures, have to be restrained against out-of-plane distortion or buckling because of their flexibility in that direction. This restraint can be provided by adding longitudinal stiffeners to the plates and the combination is well-known as a stiffened plate panel. Nowadays, stiffened plate panel forms a basic building block of many thin-walled structures.

A substantial number of investigations have been published on the strength of longitudinally stiffened steel plates in compression (see for example, Crisfield, 1975; Little, 1976; Horne and Narayanan, 1977; Webb and Dowling, 1980; Murray, 1983). Most of these studies are concerned with the strength and design of wide eccentrically stiffened plates used as compression flanges of steel box girders of built-up bridges.

In the field of cold-formed steel structures where elements of high width to thickness ratios are used, intermediate stiffeners are becoming more widely used to reduce local buckling effects in stiffened plate elements by using these stiffeners to minimise deflections at the stiffener locations. A very simple way of adding stiffeners to a stiffened plate is to form corrugations in the plate. It is often advantageous to use several such corrugations or stiffeners but even one can have a very substantial effect, and may be all that is needed. A stiffened plate by definition is supported on its longitudinal edges, and when a stiffener is added between the supports, it is known as an intermediately stiffened plate. The analysis presented here is restricted to the case of an intermediately stiffened plate with one stiffener centrally located on one side of the plate.

Research and literature publication on the behaviour of cold-formed narrow intermediately stiffened plates after critical buckling is fairly limited. Konig and Thomasson (1979) and Desmond *et al.* (1981) had conducted extensive testings to study the buckling behaviour of intermediately stiffened elements which formed the compression flanges of lipped channel sections. In both papers, the prediction of the load carrying capacity of these sections using the well-known effective width method with some modifications to the basic effective width equations was reported. In a theoretical study of interactive buckling of plated structures subject to axial compression using the theory of mode interaction and finite strip concept, Sridharan (1983) noticed that the catastrophic effects of the local-Euler buckling interaction of wide stiffened panel were not associated with the interactive buckling of a narrow intermediately stiffened plate simply supported on its edges. Only the case of a near coincident buckling of the local and overall modes was presented in his paper. Bradford (1989) used a nonlinear finite strip theory to investigate the local buckling and post-local buckling of simply supported plates with a longitudinal stiffener in combined compression and bending. The elastic post-local buckling stiffness of a longitudinally stiffened plate was shown to be enhanced by the presence of the stiffener. The stiffener studied by Sridharan and Bradford is not of the cold-formed type but a conventional outstand attached to a panel, usually by welding.

Intermediately stiffened plate elements are often used as compression flanges of cold-formed thin-walled sections. The side plates next to the stiffener, better known as sub-elements, of these plate elements can experience uniform compressional displacement for sections under bending or axial loading. For intermediately stiffened plate elements of a section, the effect of rotational restraint on the plate edges is not so pronounced and the plate can buckle into more than one half-wave buckle. For this reason, the buckling behaviour of an intermediately stiffened plate that is simply supported is not radically different from one that is rotationally restrained at its longitudinal edges. Thus, the analytical model adopted here is an intermediately stiffened plate simply supported on both longitudinal edges and the plate subelements subjected to uniform compressional displacement or loading.

Several modes of buckling are possible in a stiffened panel but for the present analysis, two modes of buckling distinctly characterize the buckling behaviour of a cold-formed narrow intermediately stiffened plate in compression. One mode involves the deflection of the stiffened plate along its length and is known as overall stiffener buckling. This is shown in Fig. 1. The second mode is when the stiffener remains straight but the plate between the edge support and the stiffener buckles in short wavelengths as shown in Fig. 2. This is known as local plate buckling. Due to the inherent nature of an eccentric stiffener, local buckling can necessarily induce overall stiffener deflections or vice-versa. The interaction of local plate and overall stiffener buckling modes in a narrow intermediately stiffened plate simply supported at all edges will be studied theoretically in this paper.

STATEMENT OF THE PROBLEM AND ASSUMPTIONS

The cross section of the intermediately stiffened plate studied is of the form shown in Fig. 3. The loaded ends are considered to be simply supported. The load is considered to be applied through the centroidal axis of the full cross section which imposes a uniform in-plane displacement of u^*. The unloaded edges are simply supported and free to move in

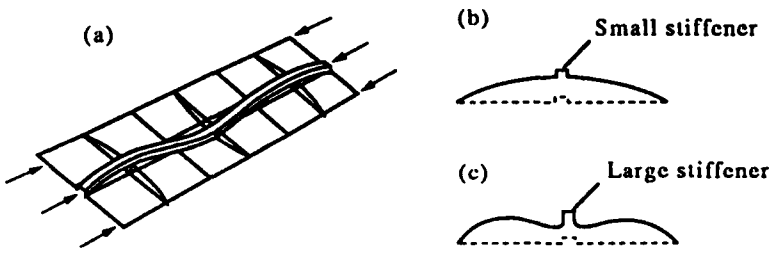

Fig. 1. Overall stiffener buckling mode.

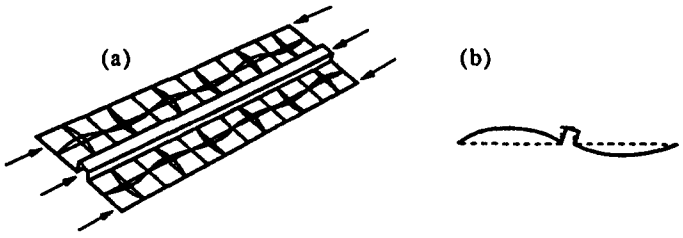

Fig. 2. Local plate buckling mode.

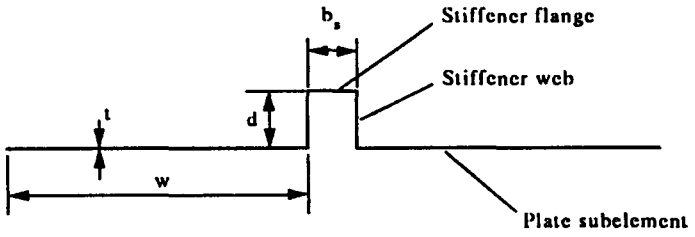

Fig. 3. Intermediately stiffened plate.

the plane of the plate, i.e. the in-plane normal stress σ_y and shear stress τ_{xy} have zero values. On the loaded edge, the shear stress τ_{xy} is considered to be zero.

Some simplifying assumptions are made so that the rather complex analysis of the behaviour of the stiffener and the plate-stiffener junction can be ignored:

1. The stiffener does not buckle locally. Therefore the strain distribution over the stiffener depth is linear.
2. Torsional stiffness of the stiffener is neglected in the consideration of local plate buckling.
3. The slope of the plate at the axis of the junction for the stiffener buckling mode is zero.

THEORETICAL ANALYSIS

The semi-energy method of analysis is essentially that first used by Marguerre (1937) and later by Rhodes and Harvey (1971) who applied it to examine the buckling behaviour of plates. In examining the buckling behaviour of intermediately stiffened elements, the possibility of plate initiated buckling (local plate buckling) and stiffener initiated buckling (overall stiffener buckling) occurring either individually or simultaneously is considered.

The theoretical analysis is described with reference to the co-ordinate system shown in Fig. 4. The section is treated as a system of thin plates, consisting of the plate subelement, stiffener web and stiffener flange, joined at the edges. The method of approach now is to

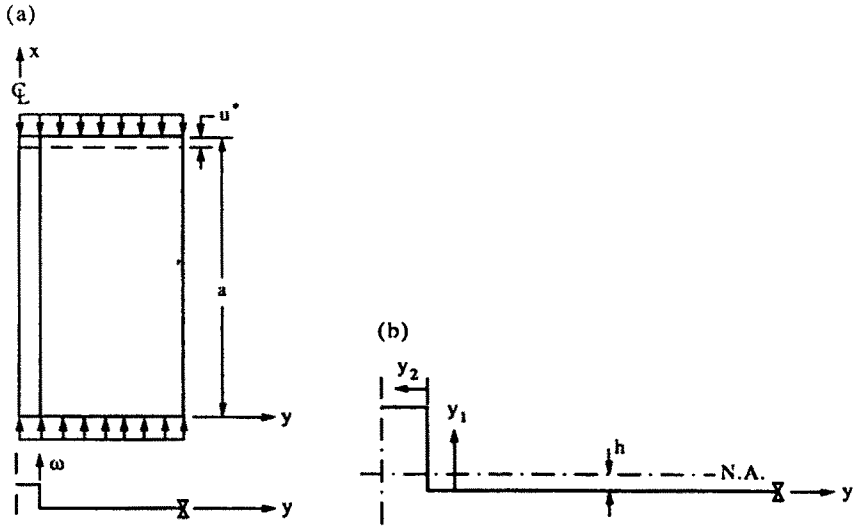

Fig. 4. Co-ordinate system.

postulate a series of deflection functions which describe the buckled form of the plate subelements and the stiffener and find the compatible stress system using von Karman's compatibility equation, to obtain the strain energies of the buckled plate and finally to utilise the principle of minimum strain energy to obtain values for the coefficients in the deflection functions. Since the plate subelements are similar and hence have the same deflected form, one half of the section is considered for convenience.

Deflection functions

The deflections of the plate subelement are assumed to be of the form:

$$\omega_p = Y(y)\sin\frac{m\pi x}{a} + Y_L(y)\sin\frac{n\pi x}{a}, \tag{1}$$

and for the stiffener,

$$\omega_s = [Y(y)]_{y=0}\sin\frac{m\pi x}{a}, \tag{2}$$

where

$$Y(y) = \sum_{N=1}^{N=2} A_N Y_N(y)$$

$$Y_L(y) = \sum_{N=1}^{N=2} B_N Y_{LN}(y), \tag{3a}$$

and

$$Y_1 = 1 + C_2\left(\frac{y}{w}\right)^2 + C_3\left(\frac{y}{w}\right)^4$$

$$Y_2 = \left(\frac{y}{w}\right)^2 + D_2\left(\frac{y}{w}\right)^3 + D_3\left(\frac{y}{w}\right)^4$$

$$Y_{L1} = \left(\frac{y}{w}\right) + K_2\left(\frac{y}{w}\right)^3 + K_3\left(\frac{y}{w}\right)^5$$

$$Y_{L2} = \left(\frac{y}{w}\right) + S_2\left(\frac{y}{w}\right)^3 + S_3\left(\frac{y}{w}\right)^4 + S_4\left(\frac{y}{w}\right)^5 + S_5\left(\frac{y}{w}\right)^6. \tag{3b}$$

In eqn (3a), A_N and B_{LN} are magnitude coefficients and m and n are the number of buckles in a stiffener and local plate buckling modes respectively in the x-direction. In eqn (3b), Y_1, Y_2, Y_{L1} and Y_{L2} are the algebraic polynomials describing the deflection form in the y-direction. Y_1 describes a predominantly stiffener buckling mode with substantial stiffener deflection while Y_2 describes the stiffener induced simultaneous symmetrical local plate buckling, the degree of influence being dependent on the flexural stiffness of the stiffener, as shown in Fig. 1(c). Y_{L1} and Y_{L2} describe the local plate deflections without stiffener deflections. Since it is well known that flat plate tends to 'flatten' out at the centre as the postbuckling range is increased, Y_{L2} is chosen to effect the local buckle waveform changes. The coefficients in the polynomial functions are evaluated through satisfying the boundary conditions at the supported edges and the plate-stiffener junctions.

The boundary conditions to be satisfied are given as follows:

At the plate-stiffener junction, the slope is zero for the stiffener buckling mode and there are no deflections for the local buckling mode, i.e.

$$\text{at } y = 0, \qquad \begin{aligned} Y_1' = Y_2' &= 0 \quad \text{for stiffener buckling} \\ Y_{L1} = Y_{L2} &= 0 \quad \text{for local buckling.} \end{aligned} \tag{4a}$$

At the unloaded edges the conditions of zero deflection and zero moment must be satisfied, i.e.

$$\text{at } y = w, \qquad \omega_p = 0$$

$$-D\left(\frac{\partial^2 \omega_p}{\partial y^2} + \nu \frac{\partial^2 \omega_p}{\partial x^2}\right) = 0. \tag{4b}$$

Note that $\partial^2 \omega_p / \partial x^2$ along the edge is zero. Applying eqn (1), it is seen that these conditions can be satisfied if:

$$\begin{aligned} Y_1 = Y_2 = Y_{L1} = Y_{L2} &= 0 \\ Y_1'' = Y_2'' = Y_{L1}'' = Y_{L2}'' &= 0. \end{aligned} \tag{4c}$$

In addition to the boundary conditions imposed at the edges of the plate subelement, two more boundary conditions were arbitrarily imposed on the local deflection function Y_{L2} at the middle of the subelement to give the deflected form shown in Fig. 5. As explained earlier, this function is chosen to effect the flattening at the centre of the plate subelement. The extra boundary conditions are zero deflection and zero slope at the centre of the subelement, i.e.

$$\text{at } y = w/2, \qquad Y_{L2} = Y_{L2}' = 0. \tag{4d}$$

The coefficients in the polynomial functions of eqn (3b) are evaluated and have the following values.

$$\begin{aligned} C_2 &= -1.2, & C_3 &= 0.2 \\ D_2 &= -1.66667, & D_3 &= 0.66667 \\ K_2 &= -1.42857, & K_3 &= 0.42857 \\ S_2 &= -22, & S_3 &= 61 \quad S_4 = -60 \quad S_5 = 20. \end{aligned}$$

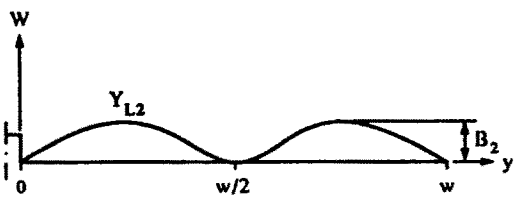

Fig. 5. Deflection function Y_{L2}.

While a two-term polynomial function has been selected for each of the buckling modes, it is assumed that in the post-local buckling range the stiffener buckle form will remain unchanged and one term is considered to be adequate. Thus only the first term A_1Y_1 and the local deflection functions are used. However, a two-term function A_NY_N i.e. A_1Y_1 and A_2Y_2 will only be used for buckling in the overall stiffener mode when there are no local plate buckles interacting with the stiffener buckles.

Solution of von Karman's compatibility equation

In the analysis of post-local buckling behaviour, the stresses in the middle surface of the subelement of width, w must satisfy the following equation, derived by von Karman, from a consideration of the compatibility of in plane and out of plane displacements:

$$\nabla^4 F = \frac{\partial^4 F}{\partial x^4} + 2\frac{\partial^4 F}{\partial x^2\,\partial y^2} + \frac{\partial^4 F}{\partial y^4} = E\left[\left(\frac{\partial^2 \omega_p}{\partial x\,\partial y}\right)^2 - \frac{\partial^2 \omega_p}{\partial x^2}\frac{\partial^2 \omega_p}{\partial y^2}\right], \tag{5}$$

where F is a stress function such that the mid-surface stresses in the plate may be obtained from its derivatives, i.e.

$$\sigma_x = \frac{\partial^2 F}{\partial y^2}, \quad \sigma_y = \frac{\partial^2 F}{\partial x^2}, \quad \tau_{xy} = -\frac{\partial^2 F}{\partial x\,\partial y}.$$

The deflections, ω_p, and in-plane stresses and displacements are related by the following formulae:

$$\varepsilon_x = \frac{\partial u}{\partial x} + \frac{1}{2}\left(\frac{\partial \omega_p}{\partial x}\right)^2, \quad \varepsilon_y = \frac{\partial v}{\partial x} + \frac{1}{2}\left(\frac{\partial \omega_p}{\partial y}\right)^2, \quad \gamma_{xy} = \frac{\partial u}{\partial y} + \frac{\partial v}{\partial x} + \frac{\partial \omega_p}{\partial x}\frac{\partial \omega_p}{\partial y}$$

and

$$\varepsilon_x = \frac{1}{E}(\sigma_x - \nu\sigma_y), \quad \varepsilon_y = \frac{1}{E}(\sigma_y - \nu\sigma_x), \quad \gamma_{xy} = 2\frac{(1+\nu)}{E}\tau_{xy}.$$

The bending action of the subelement and stiffener about the plate-stiffener combination neutral axis also gives rise to bending strains in the subelement and stiffener which are shown in Fig. 6.

It can be seen in Fig. 6 that the total strains on the plate subelement are the strain ε caused by the imposed in-plane displacement u^* and the strain caused by bending about the neutral axis, and likewise for the stiffener. Because of the assumption that the stiffener does not buckle locally and hence the linear strain and stress distribution in the stiffener, the analysis on the stiffener will be simple. The stress system on the plate subelement is more complex and the analysis will be shown here first for the subelement. To obtain the total stress system on the plate subelement after buckling, the stress system due to the in-plane displacement u^* evaluated using the von Karman's compatibility equation, will be added to the bending stress due to the bending of the stiffener.

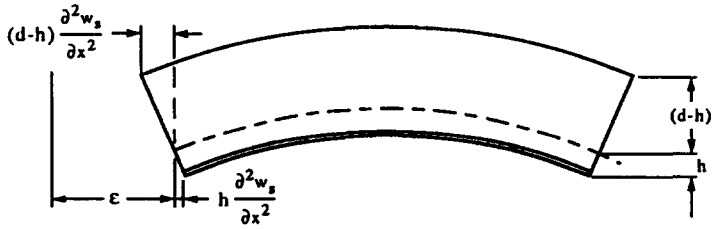

Fig. 6. Bending strains in the plate.

The corresponding stress system on the plate subelement due to in-plane displacement u^* can be obtained as follows.

Substituting one term Y_1 and two terms Y_{LN} in their expanded form into eqn (1) for ω_p and subsequently into eqn (5) gives:

$$\nabla^4 F = \frac{E\pi^2}{2a^2}\left\{m^2 A_1^2\left[(Y_1')^2 + Y_1 Y_1'' + ((Y_1')^2 - Y_1 Y_1'')\cos\frac{2m\pi x}{a}\right]\right.$$
$$+ n^2 \sum_{N=1}^{2}\sum_{M=1}^{2} B_N B_M\left[(Y'_{LN}Y'_{LM} + Y_{LN}Y''_{LM}) + (Y'_{LN}Y'_{LM} - Y_{LN}Y''_{LM})\cos\frac{2n\pi x}{a}\right]$$
$$+ \sum_{N=1}^{2} A_1 B_N[2mnY_1'Y'_{LN} + m^2 Y_1 Y''_{LN} + n^2 Y_{LN}Y_1'']\cos\frac{(n-m)\pi x}{a}$$
$$\left. + \sum_{N=1}^{2} A_1 B_N[2mnY_1'Y'_{LN} - m^2 Y_1 Y''_{LN} - n^2 Y_{LN}Y_1'']\cos\frac{(n+m)\pi x}{a}\right\}. \tag{6}$$

Thus a solution for F can be obtained in the form:

$$F = F_1 + F_2\cos\frac{2m\pi x}{a} + F_3\cos\frac{2n\pi x}{a} + F_4\cos(n-m)\frac{\pi x}{a} + F_5\cos(n+m)\frac{\pi x}{a}, \tag{7}$$

or in a simpler form,

$$F = F_1 + \sum_{i=2}^{i=5} F_i\cos e_i x, \tag{8}$$

where F_1, F_2, F_3, F_4, and F_5 can be obtained from the following equations:

$$F_1^{iv} = \frac{E\pi^2}{2a^2}\left\{m^2 A_1^2[(Y_1')^2 + Y_1 Y_1''] + n^2\sum_{N=1}^{2}\sum_{M=1}^{2} B_N B_M[Y'_{LN}Y'_{LM} + Y_{LN}Y''_{LM}]\right\}, \tag{9}$$

$$F_2^{iv} - 2\left(\frac{2m\pi}{a}\right)^2 F_2'' + \left(\frac{2m\pi}{a}\right)^4 F_2 = \frac{E\pi^2}{2a^2} m^2 A_1^2[(Y_1')^2 - Y_1 Y_1''], \tag{10}$$

$$F_3^{iv} - 2\left(\frac{2n\pi}{a}\right)^2 F_3'' + \left(\frac{2n\pi}{a}\right)^4 F_3 = \frac{E\pi^2}{2a^2} n^2 \sum_{N=1}^{2}\sum_{M=1}^{2} B_N B_M(Y'_{LN}Y'_{LM} - Y_{LN}Y''_{LM}), \tag{11}$$

$$F_4^{iv} - 2\left[(n-m)\frac{\pi}{a}\right]^2 F_4'' + \left[(n-m)\frac{\pi}{a}\right]^4 F_4$$
$$= \frac{E\pi^2}{2a^2}\sum_{N=1}^{2} A_1 B_N(2mnY_1'Y'_{LN} + m^2 Y_1 Y''_{LN} + n^2 Y_{LN}Y_1''), \tag{12}$$

$$F_5^{iv} - 2\left[(n+m)\frac{\pi}{a}\right]^2 F_5'' + \left[(n+m)\frac{\pi}{a}\right]^4 F_5$$
$$= \frac{E\pi^2}{2a^2}\sum_{N=1}^{2} A_1 B_N(2mnY_1'Y'_{LN} - m^2 Y_1 Y''_{LN} - n^2 Y_{LN}Y_1''). \tag{13}$$

Since F_1 is a function of y only, the second derivative, F_1'' which constitutes a stress in the x-direction, is the only significant part of F_1 used in the analysis. For this reason, the function F_1 itself needs not be evaluated. By integrating eqn (9) twice, F_1'' is obtained as

follows:

$$F_1'' = \frac{E\pi^2}{4a^2} m^2 A_1^2 Y_1^2 + n^2 \sum_{N=1}^{2} \sum_{M=1}^{2} B_N B_M Y_{LN} Y_{LM} + c_1 y + c_2. \tag{14}$$

The values of the constants of integration c_1 and c_2 can be obtained by examining the displacement at the end of the plate subelement.

To examine the prescribed end displacement system, take the displacement equation:

$$\varepsilon_x = \frac{\partial u}{\partial x} + \frac{1}{2}\left(\frac{\partial \omega_p}{\partial x}\right)^2.$$

The end displacement u on the plate subelement can be obtained by integrating this equation in the x-direction, i.e.

$$u = \int_0^a \left[\varepsilon_x - \frac{1}{2}\left(\frac{\partial \omega_p}{\partial x}\right)^2\right] dx. \tag{15}$$

Replacing ε_x by the corresponding stresses and noting that the periodic terms in F of eqn (7) integrate to zero, the following equation is obtained for u:

$$u = \frac{a}{E} F_1'' - \frac{a}{4}\frac{\pi^2}{a^2}\left[m^2 A_1^2 Y_1^2 + n^2 \sum_{N=1}^{2} \sum_{M=1}^{2} B_N B_M Y_{LN} Y_{LM}\right]. \tag{16}$$

Substituting for F_1'' from eqn (14) gives:

$$u = \frac{a}{E}(c_1 y + c_2). \tag{17}$$

Now the constants c_1 and c_2 can be found by considering displacement boundary conditions at the loaded ends. Since the plate subelement ends are uniformly compressed, u is a constant independent of y. Not considering the bending effects of the stiffener for the time being, the in-plane displacement u at the plate subelement is equal to the end shortening u^* applied at the centroidal axis level. Therefore,

at $x = a$,

u = constant

= u^* since $u = u^*$ (displacement due to stiffener bending will be considered later)

then

$$c_1 = 0$$

$$c_2 = -u\frac{E}{a} = -u^*\frac{E}{a},$$

i.e. c_2 is equivalent to the stress required to compress the unbuckled plate by an amount u^*. The negative sign indicates a compressive stress. (u^*/a) is equivalent to the applied strain, ε.

Therefore upon specification of an end displacement u^*, the constants c_1 and c_2 for the plate subelement are obtained and one end boundary stress condition is satisfied. The

other end boundary stress condition is that the shear stress is zero, i.e.

at $x = 0, a$

$$\tau_{xy} = -\frac{\partial^2 F}{\partial x\,\partial y} = -\left(\frac{\partial^2 F_1}{\partial x\,\partial y} - \frac{\partial^2 F_i}{\partial x\,\partial y} e_i \sin e_i x\right).$$

Since F_1 is a function of y only then $\partial^2 F_1/\partial x\,\partial y = 0$, and since m and n are integers, e_i is also an integer, then $\sin(e_i)$ equals zero at $x = 0, a$. Thus the zero shear stress condition is automatically satisfied at the loaded ends.

To solve for F_2, F_3, F_4 and F_5, substituting the functions, Y_1, Y_{L1} and Y_{L2} of eqn (3b) and their derivatives into eqns (10)–(13), a general solution for each function $F_2 - F_4$ can be obtained in the form:

$$F_2 = \frac{E\pi^2}{2a^2w^2} m^2 A_1^2 \phi_2(y), \tag{18}$$

$$F_3 = \frac{E\pi^2}{2a^2w^2} n^2 \sum_{N=1}^{2} \sum_{M=1}^{2} B_N B_M \phi_{3_{NM}}(y), \tag{19}$$

$$F_4 = \frac{E\pi^2}{2a^2w^2} \sum_{N=1}^{2} AB_N \phi_{4_N}(y), \tag{20}$$

$$F_5 = \frac{E\pi^2}{2a^2w^2} \sum_{N=1}^{2} AB_N \phi_{5_N}(y), \tag{21}$$

where ϕ_2, $\phi_{3_{NM}}$, ϕ_{4_N} and ϕ_{5_N} contain unknown constants, obtained from the complimentary function solutions of eqns (10)–(13), which are used to satisfy the stress boundary conditions at the unloaded edges and the plate-stiffener junction. The stress boundary conditions are that along the unloaded edges and plate-stiffener junction, the shear and normal stresses have zero values, i.e.

$$\frac{\partial^2 F}{\partial x\,\partial y} = \frac{\partial^2 F}{\partial x^2} = 0.$$

To avoid the display of rather long complicated expressions in the main text the evaluation of each ϕ is shown in Appendix I and it is assumed in the remainder of the text that each ϕ is known.

The stress system in the x-direction on the plate subelement can now be found by differentiating eqn (7) twice as:

$$\frac{\partial^2 F}{\partial y^2} = F'' = F_1'' + F_2'' \cos e_2 x + F_3'' \cos e_3 x + F_4'' \cos e_4 x + F_5'' \cos e_5 w$$

$$= F_1'' + \sum_{i=2}^{5} F_i'' \cos e_i x. \tag{22}$$

At this stage a solution for the stress system on the plate subelement due to in-plane displacement only has been obtained for a particular u^*. It is now necessary to consider the stresses set up by the bending of the stiffener. It can be shown from simple beam bending theory that the bending stress induced in the subelement is

$$Eh\left(\frac{\partial^2 \omega_s}{\partial x^2}\right),$$

where h is the distance from the neutral axis to the subelement mid-surface as shown in Fig. 4. The bending strains in the plate subelement and the stiffener are shown in Fig. 6.

And upon substituting of ω_s from eqn (2) and differentiating gives:

$$-Eh\left(\frac{m\pi}{a}\right)^2 A_1 \sin\left(\frac{m\pi x}{a}\right).$$

Adding to the previous eqn (22), the modified stress system in the x-direction is:

$$F'' = F_1'' + \sum_{i=2}^{5} F_i'' \cos e_i x - Eh\left(\frac{m\pi}{a}\right)^2 A_1 \sin\left(\frac{m\pi x}{a}\right). \tag{23}$$

Thus the stress system on the plate subelement is completely specified.

The stress system in the stiffener is now described. As the stiffener is assumed to have no local buckles, the periodic stress system that exists in the plate subelement does not exist in the stiffener. The strains ε_f and ε_{sf} in the stiffener web and flange respectively are simply those due to the applied strain, the membrane and bending strains set up by the deflected stiffener. The stresses in the stiffener can easily be shown to be:

For the stiffener web,

$$\sigma_s = E\varepsilon_s = E\left[\varepsilon + \frac{1}{4}\left(\frac{m\pi}{a}\right)^2 A_1^2 + \left(\frac{m\pi}{a}\right)^2 (y_1 - h) A_1 \sin\left(\frac{m\pi x}{a}\right)\right]. \tag{24}$$

For the stiffener flange,

$$\sigma_{sf} = E\varepsilon_{sf} = E\left[\varepsilon + \frac{1}{4}\left(\frac{m\pi}{a}\right)^2 A_1^2 + \left(\frac{m\pi}{a}\right)^2 (d - h) A_1 \sin\left(\frac{m\pi x}{a}\right)\right]. \tag{25}$$

The stress function F in the plate subelement and the stress in the stiffener are now completely known, and the strain energy for the stiffened plate can be evaluated in terms of the unknown coefficients A_1, B_1 and B_2 and the prescribed end displacement, u^* or strain, ε.

Evaluation of total strain energy

The elastic strain energy stored in the buckled plate subelement is the sum of that of bending, V_B, and that of in-plane stresses, V_{M_p}. These energies are given by the following expressions:

$$V_B = 2 \times \frac{D}{2} \int_0^a \int_0^w \left\{\left(\frac{\partial^2 \omega_p}{\partial x^2} + \frac{\partial^2 \omega_p}{\partial y^2}\right)^2 - 2(1-\nu)\left[\frac{\partial^2 \omega_p}{\partial x^2}\frac{\partial^2 \omega_p}{\partial y^2} - \left(\frac{\partial^2 \omega_p}{\partial x\, \partial y}\right)^2\right]\right\} dx\, dy, \tag{26}$$

$$V_{Mp} = 2 \times \frac{t}{2E} \int_0^a \int_0^w \left\{\left(\frac{\partial^2 F}{\partial x^2} + \frac{\partial^2 F}{\partial y^2}\right)^2 - 2(1+\nu)\left[\frac{\partial^2 F}{\partial x^2}\frac{\partial^2 F}{\partial y^2} - \left(\frac{\partial^2 F}{\partial x\, \partial y}\right)^2\right]\right\} dx\, dy. \tag{27}$$

The strain energy contained in the deflected stiffener is the sum of the mid-plane energies of the stiffener web and flange and they are given as follows:

$$V_{Ms} = 2 \times \frac{t}{2} \int_0^a \int_0^d \sigma_s \varepsilon_s \, dx\, dy_1 = 2 \times \frac{Et}{2} \int_0^a \int_0^d \varepsilon_s^2 \, dx\, dy_1, \tag{28}$$

$$V_{Msf} = 2 \times \frac{t}{2} \int_0^a \int_0^{b_s} \sigma_{sf} \varepsilon_{sf} \, dx\, dy_2 = 2 \times \frac{Et}{2} \int_0^a \int_0^{b_s} \varepsilon_{sf}^2 \, dx\, dy_2. \tag{29}$$

The sum of V_B, V_{Mp}, V_{Ms} and V_{Msf} now gives the total strain energy, V, in the buckled stiffened plate, i.e.

$$V = V_B + V_{Mp} + V_{Ms} + V_{Msf}. \tag{30}$$

Substitution of ω_p, F, ε_s and ε_{sf} into the energy expressions gives the strain energy in terms of the deflection magnitude coefficients, A_1, B_N and the prescribed strain ε, i.e.

$$\begin{aligned} V = K_1 A_1^4 + \sum_{N=1}^{2}\sum_{M=1}^{2}\sum_{P=1}^{2}\sum_{Q=1}^{2} B_N B_M B_P B_Q K_{2NMPQ} + [K_3\varepsilon + K_4 + K_5]A_1^2 \\ + \sum_{N=1}^{2}\sum_{M=1}^{2} B_N B_M [K_{6NM}\varepsilon + K_{7NM}] + A_1^2 \sum_{N=1}^{2}\sum_{M=1}^{2} B_N B_M K_{8NM} \\ + K_9 A_1^3 + \sum_{N=1}^{2}\sum_{M=1}^{2} A_1 B_N B_M K_{10NM} + K_{11} A_1 \varepsilon + K_{12}\varepsilon^2, \end{aligned} \tag{31}$$

where K_1, $K_{2NMPQ}, \ldots K_{11}$ and K_{12} are set out in Appendix II.

By applying the Principle of Minimum Strain Energy, the values of the deflection coefficients can be evaluated. This is done by differentiating V with respect to each coefficient (A_1, B_N) in turn and setting the derivatives to zero. Thus a set of simultaneous and nonlinear algebraic equations is obtained in the coefficients, the solution of which furnishes the values of A_1 and B_N. Due to the highly nonlinear form of the strain energy, eqn (31) is minimised using a standard minimisation routine to solve for the unknown coefficients.

Knowing the values of the coefficients corresponding to a given end displacement ε or u^*/a, it is possible to obtain expressions for the stresses and deflections at any point on the plate.

The initial buckling solution can be obtained by eliminating terms to the third power and above from eqn (31) and solving the resultant energy equation.

The total axial load acting on the stiffened plate can be obtained by integrating the longitudinal stresses over the width of the plate, i.e.

$$\begin{aligned} P &= 2 \times t\left(\int_0^w \sigma_x \, dy + \int_0^d \sigma_s \, dy_1 + \int_0^{b_s/2} \sigma_{sf} \, dy_2 \right) \\ &= 2t\left\{ \int_0^w \left(F_1'' + \sum_{i=2}^{5} F_i'' \cos e_i x - Eh\left(\frac{m\pi}{a}\right)^2 A_1 \sin\frac{m\pi x}{a} \right) dy \right. \\ &\quad + E\int_0^d \left(\varepsilon + \frac{1}{4}\left(\frac{m\pi}{a}\right)^2 A_1^2 + \left(\frac{m\pi}{a}\right)^2 (y_1 - h) A_1 \sin\frac{m\pi x}{a} \right) dy_1 \\ &\quad \left. + E\int_0^{b_s/2} \left(\varepsilon + \frac{1}{4}\left(\frac{m\pi}{a}\right)^2 A_1^2 + \left(\frac{m\pi}{a}\right)^2 (d - h) A_1 \sin\frac{m\pi x}{a} \right) dy_2 \right\}. \end{aligned} \tag{32}$$

Since the shear stress F_i' is zero at $y = 0$ and $y = w$, it can be seen that the periodic terms, $F_i \cos e_i x$ in eqn (32) integrate to zero over the plate width. As the load is independent of x, the sum of the load that varies with $\sin(m\pi x/a)$ is also zero, i.e.

$$E\left(\frac{m\pi}{a}\right)^2 \left[-hw + \left(\frac{d^2}{2} - hd\right) + (d - h)\frac{b_s}{2} \right] \sin\frac{m\pi x}{a} = 0.$$

Incidentally, the terms in the square bracket give the neutral axis of the stiffened plate.

The compressive load is now:

$$P = 2tE\left\{-\frac{u^*}{a}\left(w+\frac{b_s}{2}+d\right)+\frac{1}{4}\left(\frac{m\pi}{a}\right)^2\left[\int_0^w Y_1^2\,\mathrm{d}y+\frac{b^s}{2}+d\right]A^2 + \frac{1}{4}\left(\frac{n\pi}{a}\right)^2\sum_{N=1}^{2}\sum_{M=1}^{2}B_N B_M\int_0^w Y_{LN}Y_{LM}\,\mathrm{d}y\right\}. \quad (33)$$

Now a value of load is known for the stiffened plate corresponding to a specified end displacement. To obtain the complete post-buckling behaviour of the plate, the procedure outlined is repeated for a number of discrete increments of end displacement u^* applied to the centroidal axis.

A brief mention of analysis on overall stiffener buckling only

It has been mentioned earlier that the theoretical analysis is based on local plate initiated post-local buckling with the local plate buckles and stiffener buckles interacting at different buckle wavelengths. Plates with relatively weak stiffener will exhibit stiffener initiated post-stiffener buckling behaviour. It is possible that the instability of the stiffener will induce simultaneous symmetrical local buckles of the plate subelement of the same wavelength. In this case, the analysis is quite straight-forward, following the procedure just described. The plate deflection function will simply be:

$$\omega_p = Y(y)\sin\frac{m\pi x}{a},$$

where $Y(y)$ consists of two polynomial terms Y_1 and Y_2 found in eqn (3b).

The analysis is now complete and the behaviour of an intermediately stiffened plate can be observed theoretically. It is noted that as well as the facility of the theoretical solution to provide a continually changing buckled form throughout the post-buckling range, changes in local buckle wave-length may also be taken into account. This can be achieved by utilising the number of local buckles, n, as an additional variable parameter in the minimisation process. It is also noted that the number of buckles in the stiffener buckling mode is the one which gives the minimum buckling load with the lowest number being one. Flat plate results can also be easily obtained by simply letting the dimensions of the stiffener be zero values.

TYPICAL RESULTS

A number of theoretical results are presented here in nondimensional form. The nondimensional parameters used in the figures are defined in the Notation. The length, a, subelement width, w, and stiffener flange width, b_s, are kept constant while the thickness, t and the stiffener depth, d, are varied to show the effects of the parameters on the buckling behaviour of the stiffened plate. The plate dimensions are in millimetres.

The elastic effects of varying the stiffener depths on the load displacement behaviour of the stiffener buckling mode are shown in Fig. 7. For comparison, the behaviour of a flat plate is also shown. Since the stiffener is only on one side of the plate, two possible directions for the overall stiffener buckling must be considered, namely bowing in the direction of the stiffened side (stiffener flange in tension) and bowing in the opposite direction (stiffener flange in compression). Therefore in the figure, for each stiffener size, there are two post-buckling solutions, i.e. one with positive stiffener deflections and the other with negative deflections. The large positive deflections cause the stiffener to shed its load and the whole plate behaves like a plate without a stiffener but with an increased initial buckling load. The negative deflection curve shows similar behaviour to a cylinder under compression with the load dropping immediately after buckling and rising to equal the stiffness of the positive

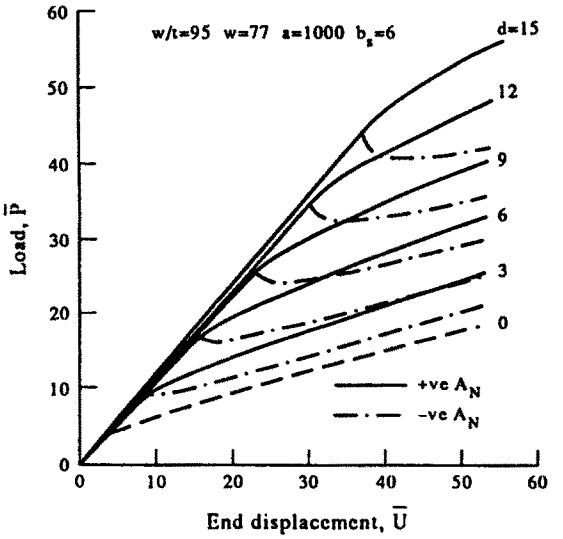

Fig. 7. Elastic post-stiffener buckling behaviour.

case in the far post-buckling range, the increase in stiffness being provided by the tensile stresses set up in the plate due to the bending of the stiffener.

In local plate buckling only, it would be expected that the addition of a stiffener will increase the initial buckling load as well as the post-buckling stiffness of the plate. The elastic behaviour of increasing the stiffener depth is shown in Fig. 8.

Figure 9 shows the post-buckling behaviour which arises on the simultaneous occurrence of both local plate and stiffener buckling modes of different buckle wavelengths compared with either the local plate buckling only or stiffener buckling only. The reduction in load from the onset of initial buckling of the interaction mode (shown by curve 2) as compared with the local buckling mode only (curve 1) is due to the deflection of the stiffener induced by local buckling. However, this interaction is not necessarily true for the stiffener initiated buckling, as shown by the lower curves of the same figure. Here, the post-buckling behaviour of a plate with a flexually weak stiffener is shown for the stiffener buckling mode with positive and negative solutions and the interaction mode. Local buckles only start to form and interact with the positive stiffener buckles, shown at point A, at loads away from the initial buckling load. It can be seen that the two curves are not significantly different from each other. In contrast, there is no interaction in the negative case.

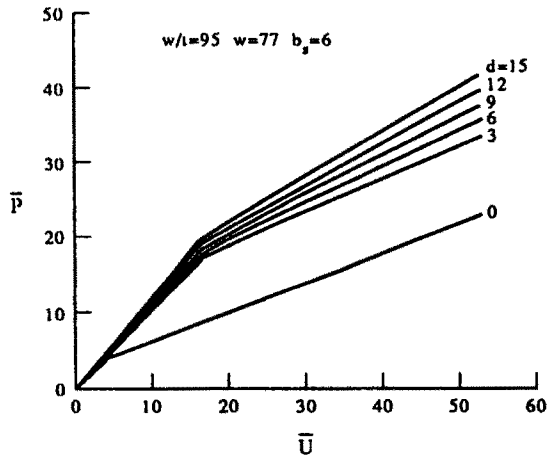

Fig. 8. Elastic post-local buckling behaviour.

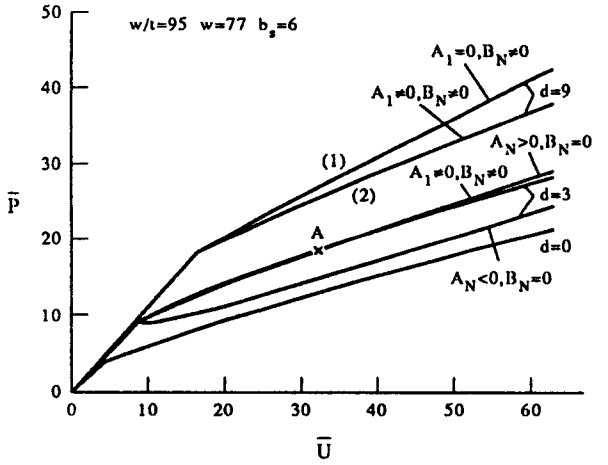

Fig. 9. Effects of interaction of overall stiffener and local plate buckling.

In view of the above observation, it will be rational, as far as the stiffener buckling mode is concerned, to assume that the stiffened plate will behave in a manner that gives the lower stiffness. Hence, the negative stiffener deflection solution is adopted for this mode.

The effects of varying the width to thickness ratio and stiffener depth on the post-buckling behaviour are shown in Figs 10–12. In Fig. 10, for a small w/t ratio of 62, stiffener buckling is the predominant buckling mode. It is interesting to note that in Figs 11 and 12 with stiffener depths of 7 and 6 mm, respectively, a sudden drop in post-buckling stiffness after point A is shown. Both stiffened plates in fact have stiffeners of sufficient rigidity against stiffener buckling but do not seem to be able to sustain their stiffness at high loads. The effect of such a stiffener with sufficient rigidity against initial stiffener buckling but not against failure by this mode is best illustrated by Fig. 13.

In Fig. 13 the local plate-initiated interaction mode is shown by curve 1. Though the stiffener buckling mode has a higher initial buckling load, its post-buckling stiffness is much lower than the interaction mode and hence the load path has to follow curve 2 at higher loads.

The influence of stiffener depths with changing buckle half wavelength in the post-buckling range is shown in Figs 14 and 15. The solid lines shown in these figures represent post-buckling solutions with the buckle wavelength taken at critical buckling while the broken lines show results with changing buckle wavelength. It is known that simply supported flat slender plates that are prone to local buckling will experience changing buckle-wavelength in the far post-buckling range if the plate aspect ratio is very high and in

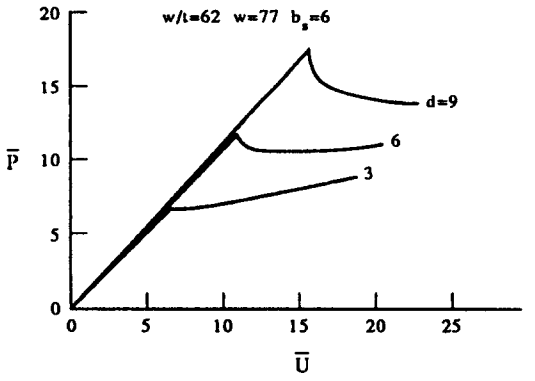

Fig. 10. Interaction buckling—low w/t ratio.

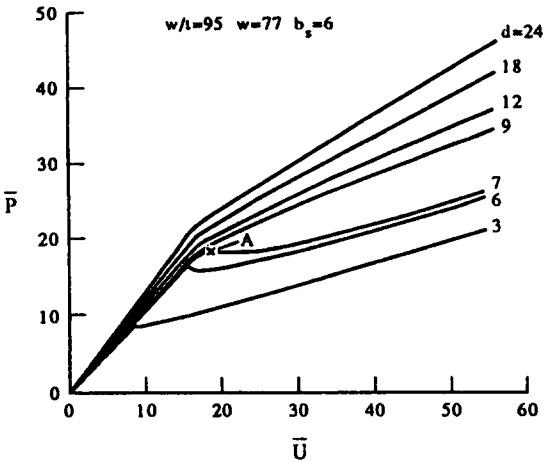

Fig. 11. Interaction buckling—medium w/t ratio.

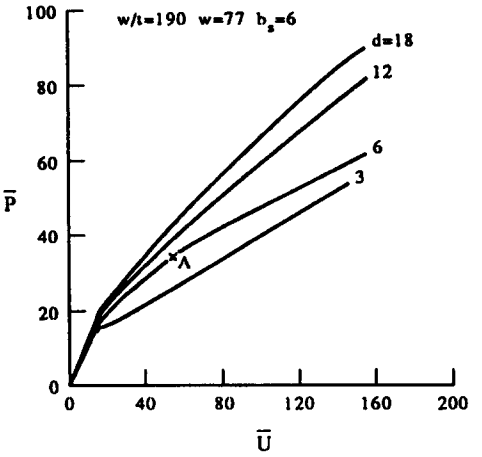

Fig. 12. Interaction buckling—high w/t ratio.

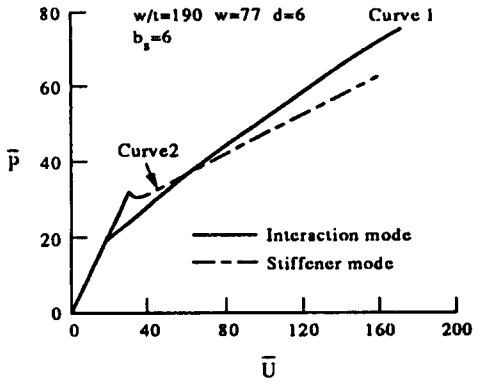

Fig. 13. Stiffener of adequate rigidity against initial buckling but not failure.

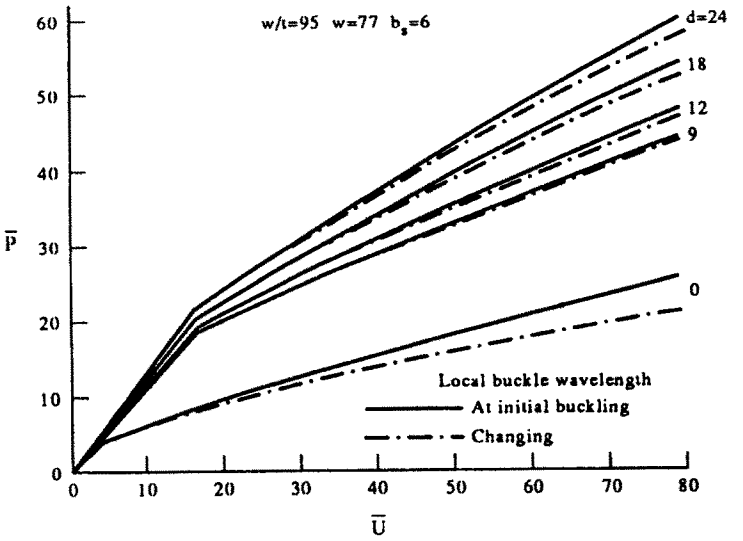

Fig. 14. Effects of changing local buckle wavelength—medium w/t ratio.

consequence a lower stiffness in this range. This effect of reducing post-buckling stiffness is shown in Figs 14 and 15 for the flat plate results. It is obvious that larger stiffener will provide adequate support to the plate subelements and these plate subelements will behave effectively as long individual simply supported plates and are therefore more susceptible to the influence of changing buckle wavelength. This is evident in Figs 14 and 15 which show that changing buckle half wavelength has a significant effect on plates having larger stiffeners at far post-buckling range.

Figure 16 shows the deflections occurring at the crest of a buckle at different load levels for the stiffener buckling mode.

The longitudinal membrane stress distributions around the section are shown in Figs 17 and 18 for the same loading magnitudes as in Fig. 16. Stresses at the node of this buckle are shown in Fig. 17 and at a crest in Fig. 18. Stresses on the stiffener are not shown on the crest as they are the same ones on the node as no local buckling is assumed to occur

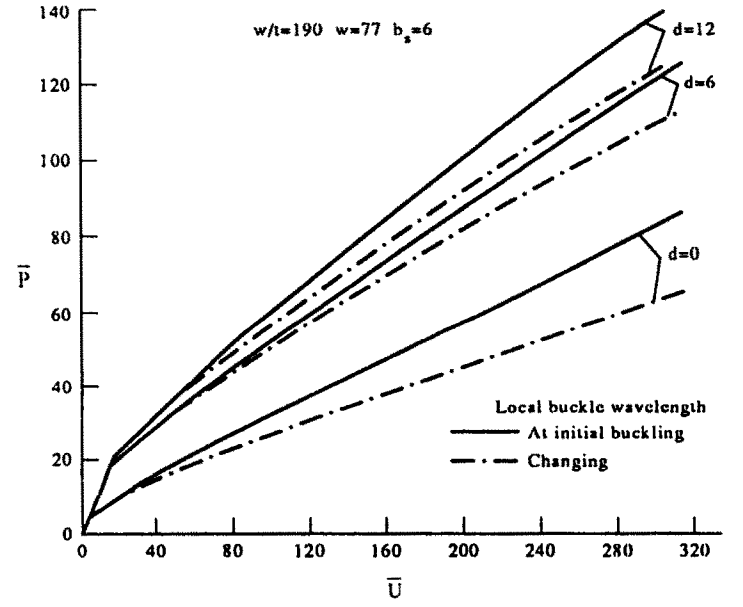

Fig. 15. Effects of changing local buckle wavelength—high w/t ratio.

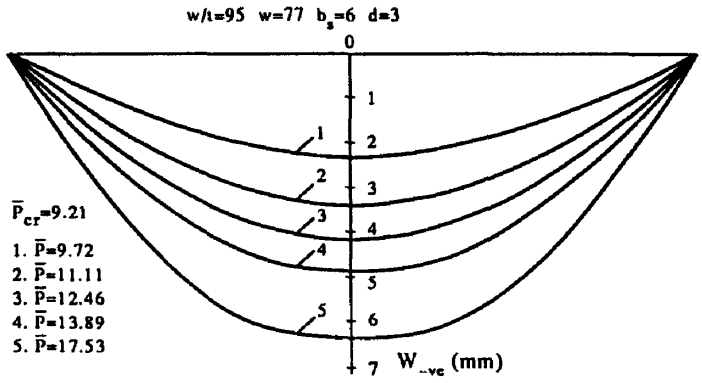

Fig. 16. Growth of deflections at crest of stiffener buckle—stiffener buckling mode.

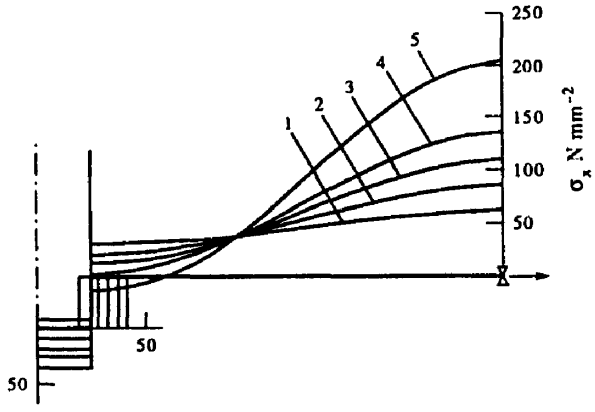

Fig. 17. Growth of membrane stress distribution at node of stiffener buckle—stiffener buckling mode.

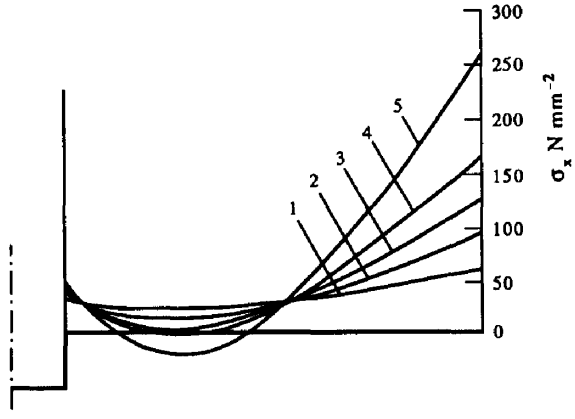

Fig. 18. Growth of membrane stress distribution at crest of stiffener buckle—stiffener buckling mode.

here. The large reductions in membrane stresses from the supported edge to the stiffener junction indicates a loss of effectiveness of this stiffener in load carrying. The stress patterns shown are very similar to that of a simply supported thin plate without a central stiffener.

Stiffener deflections occurring immediately after initial local plate buckling for a plate with a larger stiffener can be seen in Fig. 19. The membrane stress distributions at the buckle node and crest of a central local buckle for this plate are shown in Figs 20 and 21,

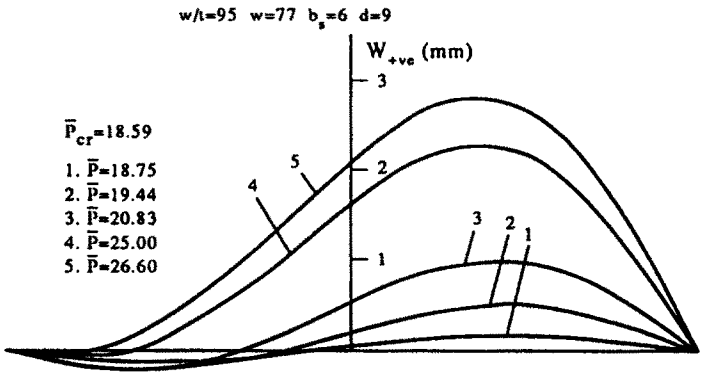

Fig. 19. Growth of deflections at crest of central local buckle—interaction buckling mode.

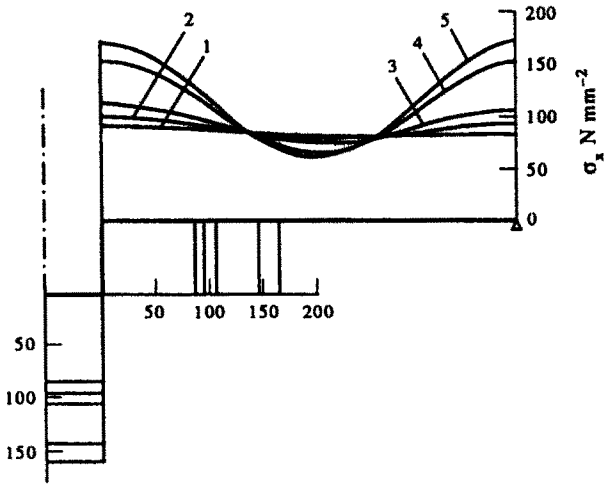

Fig. 20. Growth of membrane stress distribution at node of central local buckle—interaction buckling mode.

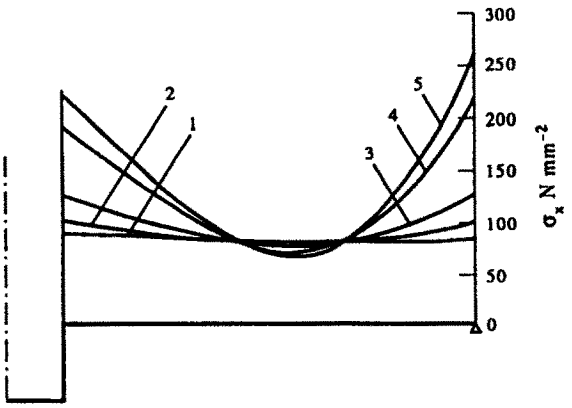

Fig. 21. Growth of membrane stress distribution at crest of central local buckle—interaction buckling mode.

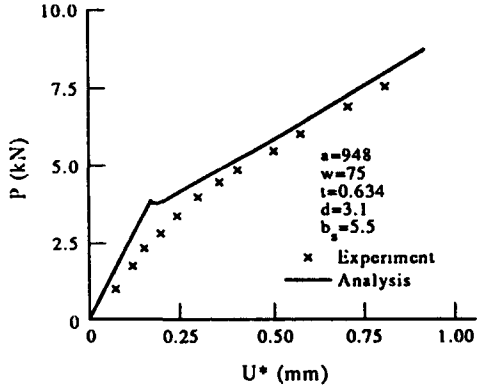

Fig. 22. Comparison of theory and test results.

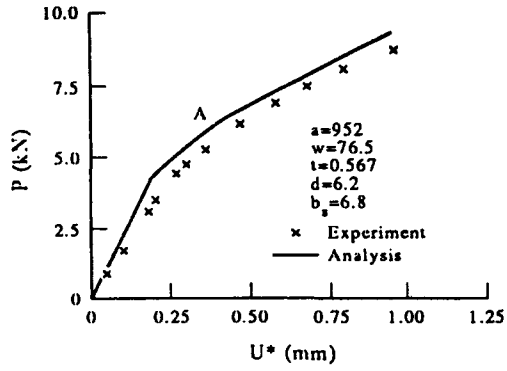

Fig. 23. Comparison of theory and test results.

respectively. The stress level at the stiffener junction is almost the same as that at the supported edge indicating the effectiveness of this stiffener to withstand high loads. Large reductions in membrane stresses in the central portion of the plate subelement are consequences of large local buckling effects on this portion.

COMPARISON WITH EXPERIMENT

A series of tests on intermediately stiffened plates was carried out to verify the validity of the analysis developed here. The method of manufacture and testing of these steel plates is described by Hoon *et al.* (1993). The test apparatus had the capability of measuring the applied load, P and the end displacement, u^*. Comparisons of the sample results of the buckling behaviours obtained from tests and those predicted by the analysis are shown in Figs 22 to 24. Figure 22 shows comparison where the stiffener is small and stiffener buckling is the predominant mode. There is a disparity between the theoretical and experimental results, especially at and around the buckling load. This disparity arises chiefly because the analysis does not take into account the initial geometric imperfections which are present in the actual plate. The current analysis can be modified to take initial imperfections into account but this will not be discussed in this paper. However, it is well-known that the effects of initial imperfections are most marked at or around the theoretical buckling load. At loads substantially greater than the buckling load, effects of imperfections on the plate behaviour are small. As can be seen in Fig. 22, the post-buckling slope of the curve for the theoretically perfect plate is more or less parallel to the experimental path. Figure 23 shows the comparison of a stiffened plate with a stiffener that offers sufficient rigidity against stiffener buckling initially but not at higher loads. The theoretical post-buckling slope is in

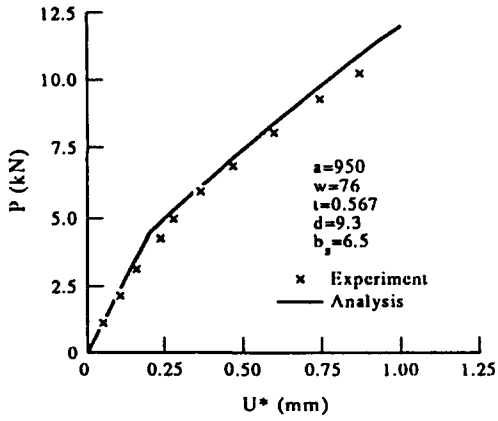

Fig. 24. Comparison of theory and test results.

fair agreement with the experimental one. Very good correlation is observed in Fig. 24 for a stiffened plate with a larger stiffener.

CONCLUSIONS

A theoretical analysis has been presented for the post-buckling behaviour of simply supported intermediately stiffened plates under uniaxial compression. Stiffener-initiated and local-plate-initiated buckling and their interaction were investigated.

A series of load-shortening curves has been given for plates with different w/t ratios and stiffener sizes, and the plate out of plane deflections and membrane stress distributions were presented for each mode of buckling. The main points arising from the results may be summarized as follows:

1. In the stiffener buckling mode, the direction of the deflected stiffener influences the plate behaviour. The worst situation occurs when the stiffener bows away from the stiffened side of the plate.
2. The use of flexurally large stiffeners retards the post-buckling deflections of the stiffeners. The onset of local plate buckling will always induce some deflections of these eccentric stiffeners.
3. A stiffener that is sufficiently rigid against stiffener buckling may not necessarily continue to resist this mode of buckling at higher loads.

Finally, the present analysis is seen to compare favourably with the experimental results.

REFERENCES

Bradford, M. A. (1989). Buckling of longitudinal stiffened plates in bending and compression. *Can. J. Civ. Engng* **16,** 607–614.

Crisfield, M. A. (1975). Full-range analysis of steel plates and stiffened platings under uniaxial compression. *Proc. ICE, Part 2* **59,** 595–624.

Desmond, T. P., Pekoz, T. P. and Winter, G. (1981). Intermediate stiffeners for thin-walled members. *Proc. ASCE, J. Struct. Div.* **107,** 627–648.

Hoon, K. H., Rhodes, J. and Seah, L. K. (1993). Tests on intermediately stiffened plate elements and beam compression elements. *Thin-Walled Structures* **16,** 111–143.

Horne, M. R. and Narayanan, R. (1977). Design of axially loaded stiffened plates. *Proc. ASCE, J. Struct. Div.* **103,** 2243–2257.

Konig, J. and Thomasson, P. O. (1979). Thin-walled C-shaped panels subjected to axial compression or to pure bending. In *Proc. Int. Confer. Thin-Walled Structures* (Edited by J. Rhodes and A. C. Walker), pp. 735–751. Granada, London.

Little, G. H. (1976). Stiffened steel compression panels—Theoretical failure analysis. *Struct. Engng* **54,** 489–500.

Marguerre, K. (1937). The apparent width of the plate in compression. NACA TM No. 833.

Murray, N. W. (1983). Ultimate capacity of stiffened plates in compression. In *Plated Structures: Stability and Strength* (Edited by R. Narayanan), pp. 135–163. Applied Science Publisher, London.

Rhodes, J. and Harvey, J. M. (1971). Plates in uniaxial compression with various support conditions at the unloaded boundaries. *Int. J. Mech. Sci.* **13,** 787–802.

Sridharan, S. (1983). Doubly symmetric interactive buckling of plated structures. *Int. J. Solids Structures* **19,** 625–641.

Webb, S. E. and Dowling, P. J. (1980). Large deflection elasto–plastic behaviour of discreetly stiffened plates. *Proc. ICE, Part 2* **69,** 375–401.

APPENDIX I

Derivation and solution of the stress function ϕ

The procedure for obtaining each ϕ is similar to that used by Rhodes and Harvey (1971) and the details are shown as follows. The procedure for solving ϕ is illustrated here for the most general function F_3. The relevant equations of F_3 are listed here for convenience and they are:

$$F_3^{iv} - 2\left(\frac{2n\pi}{a}\right)^2 F_3'' + \left(\frac{2n\pi}{a}\right)^4 F_3 = \frac{E\pi^2}{2a^2} n^2 \sum_{N=1}^{2} \sum_{M=1}^{2} B_N B_M (Y'_{LN} Y'_{LM} - Y_{LN} Y''_{LM}), \tag{A1}$$

$$F_3 = \frac{E\pi^2}{2a^2 w^2} n^2 \sum_{N=1}^{2} \sum_{M=1}^{2} B_N B_M \phi_{3_{NM}}(y). \tag{A2}$$

The deflections functions Y_{LN} can for simplicity be expressed in the general algebraic series form such that:

$$Y_{LN} = \sum_{p}^{p=r} C_{pN}\left(\frac{y}{w}\right)^p. \tag{A3}$$

Note that for all the deflection functions in eqn (3b) can be easily converted to this form.
Substituting into eqn (A1) gives:

$$F_3^{iv} - 2e_3^2 F_3'' + e_3^4 F_3 = \frac{E\pi^2}{2a^2} n^2 \sum_{N=1}^{2} \sum_{M=1}^{2} B_N B_M \sum_{p=0}^{r} \sum_{q=0}^{r} \frac{1}{w^2} C_{pN} C_{qM}[pq - q(q-1)]\left(\frac{y}{w}\right)^{p+q-2}, \tag{A4}$$

and letting $s = p+q-2$, eqn (A4) can be written simply as:

$$F_3^{iv} - 2e_3^2 F_3'' + e_3^4 F_3 = \frac{E\pi^2}{2a^2} n^2 \sum_{n=1}^{2} \sum_{M=1}^{2} B_N B_M \sum_{s=0}^{2(r-1)} \beta_{3_{sNM}} \frac{1}{w^2}\left(\frac{y}{w}\right)^s, \tag{A5}$$

where:

$$\beta_{3_{sNM}} = \sum_{0}^{q=r} C_{(s+2-q)N} C_{qM}[q(s+2-q) - q(q-1)].$$

Substituting eqn (A2) into eqn (A5) gives:

$$\phi_{3_{NM}}^{iv} - 2e_3^2 \phi_{3_{NM}}'' + e_3^4 \phi_{3_{NM}} = \sum_{s=0}^{2(r-1)} \beta_{3_{sNM}}\left(\frac{y}{w}\right)^s. \tag{A6}$$

Solving eqn (A6) gives the particular integral solution:

$$\phi_{3_{NM}} = \sum_{s=0}^{2(r-1)} \Gamma_{3_{sNM}}\left(\frac{y}{w}\right)^s \tag{A7}$$

where $\Gamma_{3_{sNM}}$ is obtained from the expression:

$$\Gamma_{3_{sNM}} = \frac{\beta_{3_{sNM}}}{e_3^4} + \frac{2(s+1)(s+2)}{w^2 e_3^2}\Gamma_{3_{(s+2)NM}} - \frac{(s+1)(s+2)(s+3)(s+4)}{w^4 e_3^4}\Gamma_{3_{(s+4)NM}}, \tag{A8}$$

$\Gamma_{3_{sNM}}$ must be evaluated from $s = 2(r-1)$ to $s = 0$ and if $s > 2(r-1)$, then $\Gamma_{3_{sNM}} = 0$.
The complementary function to equation (A6) must now be added. With this addition, the complete solution for $\phi_{3_{NM}}$ is given by:

$$\phi_{3_{NM}} = \sum_{s=0}^{2(r-1)} \Gamma_{3_{sNM}}\left(\frac{y}{w}\right)^s + C_{1_{3NM}} \cosh e_3 y + C_{2_{3NM}} \sinh e_3 y + C_{3_{3NM}}\left(\frac{y}{w}\right)\cosh e_3 y + C_{4_{3NM}}\left(\frac{y}{w}\right)\sinh e_3 y. \tag{A9}$$

The constants $C_{1_{3NM}} - C_{4_{3NM}}$ are evaluated by considering the stress boundary conditions. Satisfaction of the stress boundary conditions at the plate edges proceeds as follows.
On the unloaded edges the normal and shear stresses have zero values, i.e.

$$\frac{\partial^2 F}{\partial x^2} = \frac{\partial^2 F}{\partial x\, \partial y} = 0.$$

These conditions are satisfied if:

$$\phi_{3_{NM}} = \phi'_{3_{NM}} = 0 \quad \text{at} \quad y = w.$$

At the plate-stiffener junction, since it is assumed that the 'built-up' stiffener does not buckle locally, the stress in the stiffener is constant in the x-direction. The boundary conditions are simply that of zero normal and shear stresses at the junction. The neglect of a more rigorous boundary condition does not mean that the accuracy of the solution is greatly affected. It had been shown by Marquerre (1937) that strict adherence to the tangential stress boundary conditions makes no appreciable increase in the solution, though it has a marked effect on the values of the maximum edge stress at these edges. Therefore,

$$\phi_{3_{NM}} = \phi'_{3_{NM}} = 0 \quad \text{at} \quad y = 0.$$

By applying the boundary conditions for $\phi_{3_{NM}}$ and $\phi'_{3_{NM}}$ the constants $C_{1_{3NM}} - C_{4_{3NM}}$ are found to be:

$$C_{1_{3NM}} = -\Gamma_{0_{3NM}}$$

$$C_{2_{3NM}} = \frac{\Gamma_{1_{3NM}} T_{4_3} + \Gamma_{0_{3NM}} e_3 w \sinh e_3 w - \Sigma s\Gamma_{s_{3NM}} - T_{1_{3NM}} T_{3_3}}{e_3 w \cosh e_3 w + T_{2_3} T_{3_3} - e_3 w T_{4_3}}$$

$$C_{3_{3NM}} = -\Gamma_{1_{3NM}} - e_3 w C_{2_{3NM}}$$
$$C_{4_{3NM}} = T_{1_{3NM}} + T_{2_3} C_{2_{3NM}}. \tag{A10}$$

where

$$T_{1_{3NM}} = \left(\Gamma_{0_{3NM}} \cosh e_3 w + \Gamma_{1_{3NM}} \cosh e_3 w - \Sigma \Gamma_{s_{3NM}}\right) \Big/ \sinh e_3 w$$
$$T_{2_3} = (e_3 w \cosh e_3 w - \sinh e_3 w)/\sinh e_3 w$$
$$T_{3_3} = e_3 w \cosh e_3 w + \sinh e_3 w$$
$$T_{4_3} = e_3 w \sinh e_3 w + \cosh e_3 w. \tag{A11}$$

The solution for $\phi_{3_{NM}}$ is now complete.

Similarly, the procedure just described for solving $\phi_{3_{NM}}$ is applied to ϕ_2, ϕ_{4_N} and ϕ_{5_N} by replacing the relevant suffices in the preceding equations, for example,

$$\phi_{5_N}(y) = \sum_{s=0}^{2(r-1)} \Gamma_{5_{sN}} \left(\frac{y}{w}\right)^s + C_{1_{5N}} \cosh e_5 + C_{2_{5N}} \sinh e_5 y + C_{3_{5N}} \left(\frac{y}{w}\right) \cosh e_5 y + C_{4_{5N}} \left(\frac{y}{w}\right) \sinh e_5 y.$$

APPENDIX II

Expressions of the constants in the total strain energy expression

$$K_1 = \frac{at}{32} E \left(\frac{\pi}{a}\right)^4 2m^4 \left[\int_0^w \left(Y_1^4 + \frac{2}{w^4}(\phi_2'' - e_2^2 \phi_2)^2\right) dy + \left(\frac{b_s}{2} + d\right)\right]$$

$$K_{2NMPQ} = \frac{at}{32} E \left(\frac{\pi}{a}\right)^4 2n^4 \int_0^w [Y_{LN} Y_{LM} Y_{LP} Y_{LQ} + (\phi''_{3_{NM}} - e_3^2 \phi_{3_{NM}})(\phi''_{3_{PQ}} - e_3^2 \phi_{3_{PQ}})]\, dy$$

$$K_3 = \frac{at}{32} E \left(\frac{\pi}{a}\right)^4 \left[16 \left(\frac{am}{\pi}\right)^2 \left(\int_0^w Y_1^2\, dy + \frac{b_s}{2} + d\right)\right]$$

$$K_4 = \frac{at}{32} E \left(\frac{\pi}{a}\right)^4 \left[16m^4 \left(h^2 w + \left(h^2 d - h d^2 + \frac{d^2}{3}\right) + (h-d)^2 \frac{b_s}{2}\right)\right]$$

$$K_5 = \frac{at}{32} E \left(\frac{\pi}{a}\right)^4 \left[\frac{4}{3} \frac{t^2}{(1-\nu^2)} \left(\frac{a}{\pi}\right)^4 \int_0^w \left(Y_1'' - \left(\frac{m\pi}{a}\right)^2 Y_1\right)^2 dy\right]$$

$$K_{6NM} = \frac{at}{32} E \left(\frac{\pi}{a}\right)^4 \left[16 \left(\frac{an}{\pi}\right)^2 \int_0^w Y_{LN} Y_{LM}\, dy\right]$$

$$K_{7NM} = \frac{at}{32} E \left(\frac{\pi}{a}\right)^4 \left[\frac{4}{3} \frac{t^2}{(1-\nu)^2} \left(\frac{a}{\pi}\right)^4 \int_0^w \left(Y_{LN}'' - \left(\frac{n\pi}{a}\right)^2 Y_{LN}\right)\left(Y_{LM}'' - \left(\frac{n\pi}{a}\right)^2 Y_{LM}\right) dy\right]$$

$$K_{8NM} = \frac{at}{32} E \left(\frac{\pi}{a}\right)^4 \left\{4 \int_0^w \left[m^2 n^2 Y_1^2 Y_{LN} Y_{LM} + \frac{1}{w^4}(\phi''_{4_N} - e_4^2 \phi_{4_N})(\phi''_{4_M} - e_4^2 \phi_{4_M}) + (\phi''_{5_N} - e_5^2 \phi_{5_N})(\phi''_{5_M} - e_5^2 \phi_{5_M})\right] dy\right\}$$

$$K_9 = \frac{at}{32} E \left(\frac{\pi}{a}\right)^4 \left\{\frac{32m^3}{\pi} \left[\frac{h}{m} \int_0^w Y_1^2\, dy + \left(hd - \frac{d^2}{2}\right) + (h-d)\frac{b_s}{2} + \frac{2h}{2mw^2} \int_0^w (\phi_2'' - e_2^2 \phi_2)\, dy\right]\right\}$$

$$K_{10NM} = \frac{at}{32} E \left(\frac{\pi}{a}\right)^4 \left\{\frac{32m^2}{\pi} h \int_0^w \left[\frac{n^2}{m} Y_{LN} Y_{LM} + \frac{2mn^2}{(4n^2 - m^2)w^2}(\phi''_{3_{NM}} - e_2^2 \phi_{3_{NM}})\right] dy\right\}$$

$$K_{11} = -\frac{at}{32} E \left(\frac{\pi}{a}\right)^4 \left\{128 \left(\frac{ma}{\pi}\right)^2 \frac{1}{m\pi} \left[hw + \left(hd - \frac{d^2}{2}\right) + (h-d)\frac{b_s}{2}\right]\right\}$$

$$K_{12} = \frac{at}{32} E \left(\frac{\pi}{a}\right)^4 \left[32 \left(\frac{a}{\pi}\right)^4 \left(w + d + \frac{b_s}{2}\right)\right].$$